Shimmed matching pulses: Simultaneous control of rf and static gradients for inhomogeneity correction

John M. Franck,[1,2,3,a)] Vasiliki Demas,[2,4] Rachel W. Martin,[2,5] Louis-S. Bouchard,[2,6] and Alexander Pines[2,3]
[1]*Department of Chemistry and Biochemistry, University of California, Santa Barbara, California 93106, USA*
[2]*College of Chemistry, University of California, Berkeley, California 94720, USA*
[3]*Materials Sciences Division, Lawrence Berkeley National Laboratory, Berkeley, California 94720, USA*
[4]*T2 Biosystems, 286 Cardinal Medeiros Ave., Cambridge, Massachusetts 02141, USA*
[5]*Department of Chemistry, University of California, Irvine, California 92697, USA*
[6]*Department of Chemistry and Biochemistry, University of California, Los Angeles, California 90095, USA*

(Received 19 January 2009; accepted 16 September 2009; published online 21 December 2009)

Portable NMR systems generally suffer from poor field homogeneity and are therefore used more commonly for imaging and relaxation measurements rather than for spectroscopy. In recent years, various approaches have been proposed to increase the sample volume that is usable for spectroscopy. These include approaches based on manual shimming and those based on clever combinations of modulated radio frequency and gradient fields. However, this volume remains small and, therefore, of limited utility. We present improved pulses designed to correct for inhomogeneous dispersion across wide ranges of frequency offsets without eliminating chemical shift or spatial encoding. This method, based on the adiabatic double passage, combines the relatively larger corrections available from spatially matched rf gradients [C. Meriles *et al.*, J. Magn. Reson. **164**, 177 (2003)]. with the adjustable corrections available from time-modulated static field gradients [D. Topgaard *et al.*, Proc. Natl. Acad. Sci. U.S.A. **101**, 17576 (2004)]. We explain the origins of these corrections with a theoretical model that simplifies and expedites the design of the pulse waveforms. We also present a generalized method for evaluating and comparing pulses designed for inhomogeneity correction. Experiments validate this method and support simulations that offer new possibilities for significantly enhanced performance in portable environments. © *2009 American Institute of Physics*. [doi:10.1063/1.3243850]

I. INTRODUCTION

For many years, nuclear magnetic resonance (NMR) measurements could only be acquired with expensive, immobile laboratory instruments. In recent years, the development of portable, single-sided NMR sensors allowed the possibility for truly mobile measurements. Such sensors can be taken into the field, where they can noninvasively analyze portions of arbitrary-sized samples to acquire spin density images, as well as information on spin relaxation and motion.[1,2]

However, such mobile NMR devices attempt to extract signals from sample volumes that approach a significant fraction of the sensor's size. The sensor is typically a discrete array of permanent magnet elements and typically does not enclose the sample (i.e., it is single sided). Therefore, variations in the magnetic field hinder attempts to perform standard NMR experiments, such as chemical shift-resolved spectroscopy. Even the smaller inhomogeneities of a very cleverly designed mobile system will significantly dephase precessing nuclear spins. Although in some other circumstances, this dephasing could be ignored, it will attenuate the free induction decay (FID) signal acquired and broaden the resonances so that the spectrum becomes devoid of any chemical information.

The implementation of fully functional mobile NMR systems therefore requires a means of counteracting these inhomogeneities. Signal acquisition over a very small region can lead to homogeneous spectra;[3,4] however, many applications need the signal acquired from relatively larger volumes, especially when the rf coil is large or distant with respect to this volume (and the filling factor is low). Shim elements based on magnetic materials or electromagnetic coils can generate spatially varying fields to cancel field inhomogeneities. See, for example, previous work,[5] where the field of a mobile system was corrected to the order of less than 1 ppm across a volume on the order of tenths of a cubic centimeter. Unfortunately, additional hardware components of any kind add complexity to the design of a system and require either more power or a longer setup time. Therefore, in this article, we enhance corrective methods based on rf pulse sequences.

Methods based on rf pulse sequences will alleviate some of the need for the added design complexity and setup time (or power) required by extensive field shimming procedures or, alternatively, will relax the constraints on the hardware design needed to achieve a given level of accuracy. In con-

a)Electronic mail: johnfranck@gmail.com.

trast to the overhead required for new hardware components, most NMR spectrometers can routinely modulate the amplitude, phase, and frequency of rf pulses in order to generate new types of pulses. Various authors have shown ways of manipulating this flexibility to effect uniform rotations over wide ranges of offsets without any change to the basic hardware.[6–9] Others have directly attacked the problem of signal acquisition in inhomogeneous fields with pulse sequences that exploit the signal refocused by inversion pulses[10–12] as well as pulse sequences that employ multiple quantum coherence to remove the effects of inhomogeneities.[13–15] Recently developed "ex situ" pulse sequences,[16,17] the type of rf pulse sequences discussed in this article, focus on employing this same flexibility to selectively refocus the effects of inhomogeneities on the sample.

Ex situ pulse methods capitalize on the fact that a magnetic resonance (MR) signal consists of a series of acquisition points separated by discrete time intervals of spin evolution. Over such an interval, the inhomogeneity in the static magnetic field results in a spatially dependent rotation about the local quantization axis (z-axis). The application of an equal and opposite rotation will refocus the spins dispersed by the inhomogeneity, thus recovering signal without disturbing any chemical shift or imaging information encoded by the spins. The central challenge of ex situ NMR is the design of rf pulses that generate z-rotations proportional and opposite to the field inhomogeneity across the sample space.

From another perspective, ex situ pulses act as a sophisticated analog of imaging encoding. They can be viewed as a type of phase[18] encoding pulse, employed to cancel the undesirable encoding resulting from a period of inhomogeneous evolution; they recover signal in a fashion analogous to a gradient echo. Unlike typical phase encoding pulses, where gradient fields can only generate a spatially linear encoding, shim pulses combine gradient modulation with rf modulation to encode a phase that varies nonlinearly along one or more dimensions, while avoiding incorporating any evolution due to chemical shifts or local field offsets.

Various schemes for applying arbitrarily spatially varying phases (i.e., z-rotations) have been developed or could be adapted to this purpose, such as Shinnar–Le Roux[19] pulses in the presence of a gradient or Freeman's polychromatic pulses.[20,21] Most notably, some methods based on voxel or slice-correction strategies[20,22,23] allow for rf-based corrections of inhomogeneities and function uniquely well in combination with ultrafast NMR spectroscopy (i.e., multidimensional spectroscopy acquired in a single scan). However, if mobile sensors are to employ such rf pulses effectively, they must necessarily act uniformly across a range of offsets (field inhomogeneities and chemical shift offsets). Unlike ultrafast methods, they must also maximize signal by allowing all spins in the sample to contribute to the signal at all time points in the free induction decay. More recent developments in ex situ MR[24,25] have addressed these needs by resorting to adiabatic pulses for their insensitivity to off-resonance effects.

Therefore, in this article (as in previous work[24,25]), we focus on the design of z-rotations that operate uniformly across a wide range of offsets and that can extend easily to multiple spatial dimensions. Such corrections are uniquely suited for applications in portable systems. We describe an experiment that can explicitly demonstrate this offset robustness, and we demonstrate that the adiabatic approximation can clearly explain how such pulses give rise to complex corrections, thus simplifying and speeding up the design process. The resulting model simultaneously describes "shim pulses"[25] and "matching pulses."[24] This, in turn, allows us to generate a single pulse that incorporates the benefits of both classes of pulses into a single, powerful, and rapid corrective rotation, which acts uniformly across a wide range of offsets.

II. THEORY

In this section, we explain the differences between hardware matching and shim pulses and then review the adiabatic approximation and its implications for these pulses. With this background in hand, we then elucidate the mechanism responsible for both hardware matching and shim pulse effects in detail. We next determine how shim pulses uniformly apply a nonlinear correction across a wide range of offsets, then demonstrate how this reasoning naturally extends to incorporate hardware matching strategies. Finally, we demonstrate a simple means of spatially translating shim pulse corrections; this method will allow the optimal combination of the matching and shimming effects.

A. Hardware matching pulses versus shim pulses

In order to apply a spatially dependent corrective rotation, ex situ pulses must be able to discriminate between different locations in space. A spatially varying rf field can rotate spins differently at different locations, as can a rf pulse acting in the presence of a static field gradient. Previously designed ex situ pulses employ one of these two separate methods and exhibit one of two extremely different behaviors.

In the first extreme, "hardware matching" pulses apply a phase directly proportional to the strength of the rf field.[24] These pulses can apply relatively large phases to rapidly correct for large inhomogeneities; however, the rotation which they apply cannot actually cancel the effects of the static field inhomogeneity unless the rf and static field gradients exactly match at all points in space. When the shape of the static field inhomogeneity changes, one must either construct a new rf coil for each different field profile or employ an adjustable rf field design.[26]

Shim pulses, on the other hand, attempt to work around this rather inflexible stipulation; a time-modulated imaging gradient or a time-modulated pulsed-field gradient acts in concert with a homogeneous rf field to generate a phase that varies nonlinearly along the direction of the gradient. For example, a standard solution-state NMR probe equipped with x- and y-gradients can implement shim pulses that generate spatial corrections suitable for $\Delta B_z \propto x^2$ and x^2-y^2 inhomogeneities.[25] Changes to the time modulation of the gradient waveforms, achieved merely by reprogramming the spectrometer, alter the spatial variation in the resulting correction. However, because the corrective angle does not scale

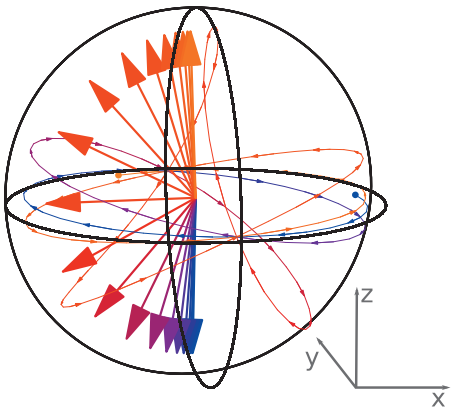

FIG. 1. A schematic representation of the effective magnetic field (bold arrows) and evolution pattern of one spin (fine line) over the course of an AFP. Time increases from blue to orange. The spins precess through a complicated trajectory, but always remain locked perpendicular to the effective field.

linearly with the gradient strength, shim pulses generate a much weaker correction than hardware matching pulses.[27]

The combined approach presented here broadens the applicability of ex situ NMR. The more efficient hardware matching provides the bulk of the corrections, while shim pulses fine tune the corrective phases to tweak the corrections to high accuracy. This is analogous to the way a typical superconducting magnet employs cryoshims and room-temperature shims. Neither alone provides a correction suitable for obtaining spectroscopy in all cases due to limitations in either the accuracy or the strength of the applied correction, while together, they apply a correction both strong and accurate. The dramatic nature of this effect will be fully demonstrated in Sec. V.

B. Adiabaticity

Both shim pulses[25] and the most robust hardware matching pulses[24] employ altered forms of the adiabatic full passage (AFP). During an AFP, both the frequency and amplitude of the rf irradiation change in time, according to the (normalized, unitless) functions $\mathcal{F}(t)$ and $\mathcal{A}(t)$, respectively. This sweeps the effective magnetic field from the z-axis, through the transverse plane, and to a final position antiparallel to its starting position. If the direction of the effective field reorients slowly, relative to its associated Larmor frequency, such that

$$\left|\frac{d}{dt}\arctan\left(\frac{B_{\mathrm{eff},z}}{B_{\mathrm{eff},x}}\right)\right| / \gamma|\mathbf{B}_{\mathrm{eff}}| \ll 1, \tag{1}$$

where $B_{\mathrm{eff},x}$ and $B_{\mathrm{eff},z}$ give the x and z components of the effective field in the rotating frame, the pulse is adiabatic. Spins initially in the transverse plane will then remain locked in the plane perpendicular to the effective field (i.e., the transverse plane of the "doubly rotating frame"[28]), even as the effective field changes direction. While in that plane, the spins rotate about the effective field $\mathbf{B}_{\mathrm{eff}}$ at its associated Larmor frequency $\gamma|\mathbf{B}_{\mathrm{eff}}|$ (Fig. 1). Thus, across a certain offset bandwidth (generally only slightly smaller than the range of the frequency modulation ω_{sw}) where it acts adiabatically, an adiabatic passage behaves in a remarkably simple and uniform fashion.

The net frequency offset $\gamma B_{\mathrm{eff},z}$ has contributions from the local resonance offset Ω and the applied gradient field $\mathbf{r}\cdot\mathbf{G}$, as well as the changing frequency of the rf pulse $\omega_{\mathrm{sw}}\mathcal{F}(t)$,

$$\gamma B_{\mathrm{eff},z} = \gamma\mathbf{r}\cdot\mathbf{G}(t) + \Omega - \omega_{\mathrm{sw}}\mathcal{F}(t). \tag{2}$$

Meanwhile, $B_{\mathrm{eff},x}$ is determined by the maximum amplitude of the rf field across both space and time $B_{1,\max}$ and varies both across space, as determined by $\Delta B_1(\mathbf{r})/B_{1,\max}$ (the spatially dependent rf misset), and as a function of time, as determined by $\mathcal{A}(t)$,

$$B_{\mathrm{eff},x} = \left(1 - \left(\frac{\Delta B_1(\mathbf{r})}{B_{1,\max}}\right)\right)B_{1,\max}\mathcal{A}(t). \tag{3}$$

The previously described behavior of an adiabatic passage now indicates that the spins will invert and experience a net rotation about the z-axis (i.e., phase) given by

$$\begin{aligned}\varphi(\mathbf{r},\Omega) &= \gamma\int_0^{t_p} |\mathbf{B}_{\mathrm{eff}}(\mathbf{r},\Omega,t)|dt \\ &= \gamma\int_0^{t_p} \sqrt{B_{\mathrm{eff},x}^2\left(\frac{\Delta B_1(\mathbf{r})}{B_{1,\max}},t\right) + B_{\mathrm{eff},z}^2(\mathbf{r},\Omega,t)}dt.\end{aligned} \tag{4}$$

Note that this approximation dramatically simplifies the calculation of the effect of the rf irradiation; without this simplification, the product of hundreds of matrices would be needed to approximate the same result.[25] Furthermore, the adiabatic approximation [Eq. (4)] provides a sufficient description of these pulses; while it may initially seem desirable to account for deviations from adiabatic behavior, such deviations will typically be undesirable, as they will prevent proper inversion of the spins and will lead to signal loss.

Although adiabatic pulses exhibit a uniquely uniform behavior that is easy to describe, neither the inversion nor the offset dependence of the phase effected by a single adiabatic passage is desired in ex situ pulses. However, when two identical AFPs act in sequence, the undesirable offset dependence and magnetization inversion cancel.[29] Therefore, adiabatic rf matching pulses, shim pulses, and the new pulses presented here are all, in fact, modifications of such an "adiabatic double passage" (ADP). In these modified versions, the two full passages differ slightly and do not completely cancel, leaving a net phase of

$$\begin{aligned}\varphi = \gamma\int_0^{t_p} \sqrt{(B_{\mathrm{eff},x}^{(2)})^2 + (B_{\mathrm{eff},z}^{(2)})^2}dt \\ - \gamma\int_0^{t_p} \sqrt{(B_{\mathrm{eff},x}^{(1)})^2 + (B_{\mathrm{eff},z}^{(1)})^2}dt,\end{aligned} \tag{5}$$

where (1) and (2) superscripts label the two consecutive passages.

C. Shim pulse

The application of gradient waveforms during an adiabatic rf pulse will, in general, cause a complicated, spatially

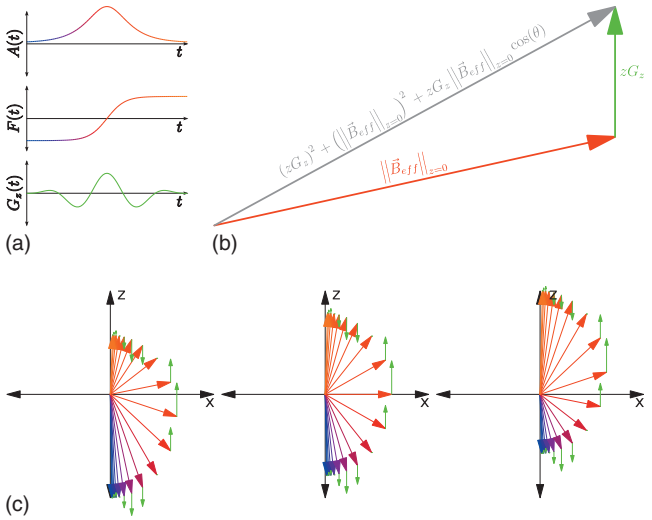

FIG. 2. Here, a gradient waveform (green), whose magnitude will scale proportionally to its position in space, adds to the effective field of an AFP (blue through orange). The gradient field will perturb the magnitude of the effective field, and therefore the adiabatic precession frequency, as shown in (b). This perturbation is a nonlinear function of **r**, which allows for the complicated spatial dependence of the phase applied by shim pulses. Such a modified adiabatic passage will apply a net phase proportional to the sum of the net effective field at all time points during the pulse. (c) illustrates the nature of this process for three different isochromats. This schematic makes it possible to see how the higher order spatial dependence for each offset is necessarily different, and why constraining the perturbation to smaller values, and therefore lower order spatial dependence, is a sensible scheme. (Note that the coordinates indicated in the figures are in the rotating frame.)

dependent change to the phase applied by the rf pulse. However, this complicated dependence has a simple origin. The above analysis [Eqs. (2)–(5)] calculates the change in phase by means of simple vector addition of the applied gradient—a spatially dependent z-vector—to the effective field. When the effective field lies along the z-axis, the application of a gradient field will simply cause the adiabatic precession frequency (i.e., the effective field Larmor frequency) to change linearly across space. More interestingly, when the gradient field adds to an effective field already tilted away from the z-axis, the adiabatic precession frequency will change according to a nonlinear function of **G** and **r** [Fig. 2(b)]. We will focus on the characterization and optimization of this nonlinear response to the applied gradient, which gives shim pulses their unique properties.

In order to compensate for evolution in highly inhomogeneous environments, shim pulses must also apply this phase uniformly across a wide range of resonance offsets. Since a pulse acting in the presence of a constant gradient cannot distinguish between intentional variations in the static field that identify different spatial positions[30] and unintentional variations due to the local field offset, this means the applied gradient amplitudes must change over time. Only pulses employing a gradient amplitude that varies over time can exhibit a different functional dependence on **r** versus Ω. Independent modulation of the different gradients will similarly decouple the x, y, and z dependences. This simple trick has, to our knowledge, only been applied in one previous example.[25]

Although gradient modulation thus allows for extraordinary flexibility, it also poses a problem. The net effective field strengths corresponding to different offset isochromats must necessarily depend differently on the spatial coordinates [see Fig. 2(c)]. In order to develop a useful solution, one must minimize this complicated interaction between the offset and spatial dependences.

Therefore, we examine a regime where the gradients perturbatively affect the resulting phase. Two facts support this choice. In the limit of very large gradient fields (approaching the strength of the effective field), large changes to the z component of the effective field will prevent the slow reorientation of the effective field and disrupt the adiabatic inversion of the spins, thus rendering the pulses useless. Meanwhile, in the opposite extreme, the phase will respond linearly to the application of a gradient—of any time dependence—whose magnitude approaches zero, and will therefore only exhibit a linear spatial dependence. The intermediate, perturbative approach represents a good compromise since it can simplify the spatial and offset dependences, separate them into a limited number of terms, and adjust the relative magnitude of these terms to generate corrections shaped similarly to those of a shim stack.

The Taylor–Maclaurin expansion of Eq. (4) expresses this idea more concretely. This expansion,

$$\varphi(\mathbf{r},\Omega)=\sum_{n_\Omega=0}^{\infty}\sum_{n_x=0}^{\infty}\sum_{n_y=0}^{\infty}\sum_{n_z=0}^{\infty}\left(\frac{\partial^{n_\Omega}}{\partial\Omega^{n_\Omega}}\frac{\partial^{n_x}}{\partial x^{n_x}}\frac{\partial^{n_y}}{\partial y^{n_y}}\frac{\partial^{n_z}}{\partial z^{n_z}}\varphi(\mathbf{r},\Omega)\bigg|_{\mathbf{r}=\Omega=0}\frac{\Omega^{n_\Omega}x^{n_x}y^{n_y}z^{n_z}}{n_\Omega!\,n_x!\,n_y!\,n_z!}\right), \tag{6}$$

breaks the spatial and offset dependence of the phase into a sum of monomials of r_i and Ω. Specifically, the monomial term f of orders n_i in space and order n_Ω in local offset will be

$$f(\mathbf{r},\Omega)=\gamma\frac{c_f}{t_f}\left(\frac{\Omega}{\gamma}\right)^{n_\Omega}x^{n_x}y^{n_y}z^{n_z},$$

where

$$t_f=n_\Omega!\,n_x!\,n_y!\,n_z!\,,$$

$$c_f=\int_0^{t_p}\left[\frac{\partial^N|\mathbf{B}_{\mathrm{eff}}|}{\partial B_{\mathrm{eff},z}^N}\bigg|_{\mathbf{r}=\Omega=0}G_x^{n_x}G_y^{n_y}G_z^{n_z}\right]dt, \tag{7}$$

$$N = n_\Omega + n_x + n_y + n_z,$$

and we have noted that $B_{\text{eff},z}$ is linear with respect to all the gradient fields. We choose smaller gradient amplitudes, such that the coefficients c_f corresponding to high-order interactions between the gradient and the offset will vanish. The coefficients c_f for the remaining lower order monomial terms reduce to simple overlap integrals between the corresponding gradient waveforms and the response functions $\partial^N|\mathbf{B}_{\text{eff}}|/\partial B^N_{\text{eff},z}|_{\mathbf{r}=\Omega=0}$, corresponding to the net order N of the monomial. For example,

$$\begin{aligned} c_{z^2} &= \int_0^{t_p} \left.\frac{\partial^2|\mathbf{B}_{\text{eff}}|}{\partial B^2_{\text{eff},z}}\right|_{\mathbf{r}=\Omega=0} G_z^2(t)dt, \\ c_{z\Omega} &= \int_0^{t_p} \left.\frac{\partial^2|\mathbf{B}_{\text{eff}}|}{\partial B^2_{\text{eff},z}}\right|_{\mathbf{r}=\Omega=0} G_z(t)dt, \\ c_{xy} &= \int_0^{t_p} \left.\frac{\partial^2|\mathbf{B}_{\text{eff}}|}{\partial B^2_{\text{eff},z}}\right|_{\mathbf{r}=\Omega=0} G_x(t)G_y(t)dt, \\ c_{z^3} &= \int_0^{t_p} \left.\frac{\partial^3|\mathbf{B}_{\text{eff}}|}{\partial B^3_{\text{eff},z}}\right|_{\mathbf{r}=\Omega=0} G_z^3(t)dt. \end{aligned} \tag{8}$$

Therefore, the calculation of only a handful of response functions will provide a direct mapping between the gradient waveforms and the monomials that make up the corrective phases. (Note that only two response functions yield four coefficients above.)

As covered Secs. III and IV, by forcing undesirable monomial terms to vanish, one can eliminate most of the offset dependence or other undesired lower order contributions. This procedure can tailor appropriate corrective phases for a variety of different inhomogeneities.

D. Incorporation of rf matching effects

An adiabatic hardware matching pulse differs from a typical ADP in that a multiplicative factor ζ perturbs the rf amplitude of one of the adiabatic passages,[24] changing the net x component of the effective field from Eq. (3) to

$$B_{\text{eff},x} = (1+\zeta)\left(1 - \frac{\Delta B_1(\mathbf{r})}{B_{1,\max}}\right)\mathcal{A}(t)B_{1,\max}. \tag{9}$$

Figure 3 provides a geometrical illustration of how the perturbation applied by the pulse scaling will add to the effective field in a primarily linear fashion.

An adiabatic hardware matching pulse will therefore apply a phase with a spatial dependence of the form[31]

$$\varphi(\mathbf{r}) = \varphi(0) - \gamma\zeta\frac{\Delta B_1(\mathbf{r})}{B_{1,\max}}c_{\zeta\Delta B_1} + O\left(\zeta^2\frac{\Delta B_1}{B_{1,\max}}\right). \tag{10}$$

Reasoning parallel to that which leads to Eq. (8) will also give the coefficient for the dominant hardware matching monomial

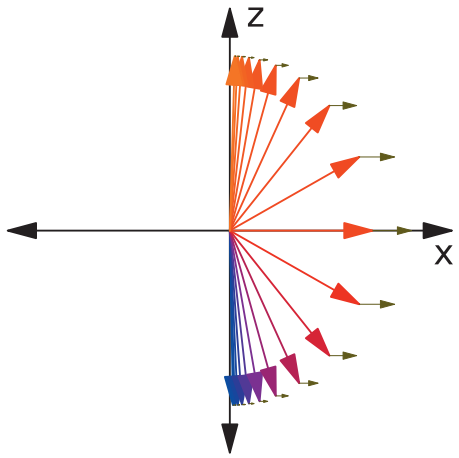

FIG. 3. Here, scaling of the rf waveform generates a change to the effective field $\zeta(1-\Delta B_1(\mathbf{r})/B_{1,\max})B_{1,\max}\mathcal{A}(t)$, illustrated by the brown arrows. Note how, especially in the low scaling limit, the change in the effective field magnitude will be primarily linear.

$$c_{\zeta\Delta B_1} = B_{1,\max}\int_0^{t_p} \left.\frac{\partial|\mathbf{B}_{\text{eff}}|}{\partial B_{\text{eff},x}}\right|_{\zeta=\Delta B_1=0} \mathcal{A}(t)dt. \tag{11}$$

As the dominant monomial scales linearly with the rf gradient, it will produce a larger effect than the second (and higher) order effects that shim pulses are designed to produce.

We must address two practical concerns in order to complete the derivation of the theory that leads to combined shimmed matching pulses. First, shimmed matching pulses will be applied in the presence of an inhomogeneous rf field, and the shim pulse portion of the phase applied must therefore exhibit insensitivity to rf misset (i.e., miscalibration or spatial inhomogeneity of the rf) as well as offset. For this purpose, we will view $\Delta B_1/B_{1,\max}$ as an rf misset parameter and eliminate spatial-mismatch cross terms (Table II) in the same fashion we eliminate spatial-offset terms [Eq. (8) and Table I]. In Sec. IV we have also restricted the gradient

TABLE I. Sample set of orthogonalization that generates a z^2 shim pulse waveform. In order to zero the coefficient in the left column, the waveform in the middle column is made orthogonal to the function in the right column. Note that both the middle and right columns are functions of time only.

Coefficient	Gradient waveform	Orthogonal to
c_y	G_y	$\frac{\partial\|\mathbf{B}_{\text{eff}}\|}{\partial B_{\text{eff},z}}$
c_x	G_x	$\frac{\partial\|\mathbf{B}_{\text{eff}}\|}{\partial B_{\text{eff},z}}$
$c_{y\Omega}$	G_y	$\frac{\partial^2\|\mathbf{B}_{\text{eff}}\|}{\partial B^2_{\text{eff},z}}$
$c_{x\Omega}$	G_x	$\frac{\partial^2\|\mathbf{B}_{\text{eff}}\|}{\partial B^2_{\text{eff},z}}$
c_{xy}	G_x	$G_y\frac{\partial^2\|\mathbf{B}_{\text{eff}}\|}{\partial B^2_{\text{eff},z}}$
$c_{xy\Omega}$	G_x	$G_y\frac{\partial^3\|\mathbf{B}_{\text{eff}}\|}{\partial B^3_{\text{eff},z}}$

waveform to only one of the adiabatic passages; this prevents the appearance of unwanted shim-matching cross terms.

E. Coordinate translation

Previously,[25] shim pulse corrections were centered about the point where the applied gradient fields pass through zero. However, in many practical cases, a shimmed matching correction will function far more optimally with the gradient-generated portion of the correction centered about a different point. Specifically, a translation of the center of the spatial coordinates by $\mathbf{c}$ would result in a z component of the effective field of the form

$$\gamma B_{\mathrm{eff},z} = \Omega + \gamma(\mathbf{r}-\mathbf{c})\cdot\mathbf{G}(t) - \omega_{\mathrm{sw}}\mathcal{F}(t)$$
$$= \Omega + \gamma\mathbf{r}\cdot\mathbf{G}(t) - \underbrace{(\omega_{\mathrm{sw}}\mathcal{F}(t) + \gamma\mathbf{c}\cdot\mathbf{G}(t))}_{\text{new frequency modulation}}. \quad (12)$$

Therefore, by augmenting the frequency modulation function of the rf pulse by $\gamma\mathbf{c}\cdot\mathbf{G}(t)$, one can translate the center of the spatial coordinates by $\mathbf{c}$. This shift in the position of the applied gradient-derived shimming phases relative to the rf gradient-derived matching phases allows the generation of a very wide variety of resulting phase profiles. Addition of a shimming correction to a matching correction can now produce not just one, but a variety of differently shaped corrective phases.

III. PULSE OPTIMIZATION

As the first step of the optimization of a new shim pulse or shimmed matching pulse, we chose an appropriate ADP sequence. In the examples shown here, we adjusted the parameters of a sech/tanh ADP to yield a compromise between a reasonably short pulse length given the available rf power and a broadband double inversion with limited residual phase (i.e., high fidelity). More information on the operation and optimization of adiabatic passages has been described in detail elsewhere.[8,28]

The actual calculation of shim and shimmed hardware matching pulses reduces to a simple, rapid procedure. The first order response functions in Eq. (7) are given by

$$\frac{\partial|\mathbf{B}_{\mathrm{eff}}|}{\partial B_{\mathrm{eff},z}} = B_{\mathrm{eff},z}I,$$

$$\frac{\partial|\mathbf{B}_{\mathrm{eff}}|}{\partial B_{\mathrm{eff},x}} = B_{\mathrm{eff},x}I, \quad (13)$$

where $I=|\mathbf{B}_{\mathrm{eff}}|^{-1}=1/\sqrt{B_{\mathrm{eff},x}^2+B_{\mathrm{eff},z}^2}$. We then group each subsequent higher order response function into a product of I and a term R, which contains some polynomial of lower order response functions. Simple algebraic manipulations will then demonstrate the recursion relations

$$\frac{\partial(RI^n)}{\partial B_{\mathrm{eff},z}} = I\left[\frac{\partial R}{\partial B_{\mathrm{eff},z}}I^{n-1} - nB_{\mathrm{eff},z}I(RI^n)\right], \quad (14)$$

TABLE II. Example of orthogonalization used to generate insensitivity to mismatch (analogous to Table I).

Coefficient	Gradient waveform	Orthogonal to
$c_{x\Delta B_1}$	G_x	$\mathcal{A}\frac{\partial^2\lvert\mathbf{B}_{\mathrm{eff}}\rvert}{\partial B_{\mathrm{eff},z}\partial B_{\mathrm{eff},x}}$
$c_{y\Delta B_1}$	G_y	$\mathcal{A}\frac{\partial^2\lvert\mathbf{B}_{\mathrm{eff}}\rvert}{\partial B_{\mathrm{eff},z}\partial B_{\mathrm{eff},x}}$
$c_{x\Delta B_1\Omega}$	G_x	$\mathcal{A}\frac{\partial^3\lvert\mathbf{B}_{\mathrm{eff}}\rvert}{\partial^2 B_{\mathrm{eff},z}\partial B_{\mathrm{eff},x}}$
$c_{y\Delta B_1\Omega}$	G_y	$\mathcal{A}\frac{\partial^3\lvert\mathbf{B}_{\mathrm{eff}}\rvert}{\partial^2 B_{\mathrm{eff},z}\partial B_{\mathrm{eff},x}}$
$c_{xy\Delta B_1}$	G_y	$G_x\mathcal{A}\frac{\partial^3\lvert\mathbf{B}_{\mathrm{eff}}\rvert}{\partial^2 B_{\mathrm{eff},z}\partial B_{\mathrm{eff},x}}$

$$\frac{\partial(RI^n)}{\partial B_{\mathrm{eff},x}} = I\left[\frac{\partial R}{\partial B_{\mathrm{eff},x}}I^{n-1} - nB_{\mathrm{eff},x}I(RI^n)\right], \quad (15)$$

which rapidly provide the analytical expressions for various response functions.

The calculation of these functions allows the algorithm to eliminate the undesirable monomial terms first order in one or more of the gradient waveforms, thus rapidly optimizing the waveform. Specifically, Gram–Schmidt orthogonalization chooses gradient waveforms orthogonal to the remainder of the appropriate integral expression in Eq. (7). For example, to generate a correction suitable for an x^2+y^2 inhomogeneity, the computer algorithm will zero all the dominant monomial terms except the x^2 and y^2 terms by choosing gradient waveforms orthogonal to functions listed in Table I. In a similar manner, orthogonalization can also remove the mismatch terms (Table II). If one wishes to effect only a partial elimination of a certain monomial, a properly scaled version of the waveform orthogonalized against (column 3 of Tables I and II) can then be added to the result of the orthogonalization procedure.

Finally, we note that the second-order spatial term for a given adiabatic passage is always positive. Therefore, the most trivial example of a third-order shim pulse will employ properly orthogonalized gradient waveforms on both adiabatic passages with an identical magnitude but opposite sign.

Once it incorporates all the features previously mentioned, the entire optimization procedure takes the following form:

(1) Optimize an unmodified sech/tanh ADP.
(2) Calculate analytical expressions for a limited number of lower order response functions.
(3) Use Eq. (14) and (15) to generate a table of discretized response functions, as in Tables I and II, column 3.
(4) Generate "orthogonal waveforms" by orthogonalizing functions in the second column of Tables I and II against functions in third column.
(5) To achieve limited but nonzero coefficients in Tables I and II, the gradient waveform consists of a weighted sum of the orthogonal waveform and a "nonorthogonal waveform" proportional to the third column.

(6) For third-order corrections, duplicate waveforms across both passages and negate one.
(7) Solve algebraic equations to scale the orthogonal and nonorthogonal components of all gradient waveforms and achieve the desired relative weighting of the monomial coefficients of interest.
(8) Add the appropriate gradient waveforms to the frequency modulation waveform to effect any desired coordinate translation, as in Eq. (12).

With computer software such as MATLAB (The Mathworks, Natick, MA), the calculation of the desired waveforms and generation of appropriate spectrometer waveform files takes only seconds. Finally, a simulation of the time evolution was performed to test the gradient waveform generated in this fashion.

IV. EXPERIMENTS

A. One-dimensional example

A sample of 10% (by volume) isopropyl alcohol in D_2O was placed in a 5 mm NMR tube inserted in a Bruker 7 T magnet operated with a Bruker Avance 300 MHz spectrometer. The rf power corresponded to a proton nutation frequency of approximately 25 kHz. The probe had been modified so that the center of the rf coil was slightly offset with respect to the center of z-axis gradient coils.

We tested the corrective phase applied by these pulses with a novel analog of a field-mapping experiment. As a faster alternative to a full phase-encoding experiment,[25] three experiments were run. In the first experiment, a precession interval separated the two adiabatic passages of a shimmed matching pulse. This generated an adiabatic echo; an approximately 5 G/cm frequency encoding gradient encoded the resulting signal, as shown in Fig. 4(b). In the second, "baseline image" experiment, an unaltered ADP acted as the adiabatic echo pulse; the signal was frequency encoded but has no net z-rotation applied by the pulse. Throughout these experiments, the isopropanol spectrum provided spins with primarily two different frequencies for each point in space. These allowed a limited demonstration of the pulse robustness, but interfered with the frequency encoding. Therefore, the third and final experiment provided a spectral baseline; neither frequency encoding gradients during acquisition nor any net z-rotation applied by the ADP influenced the signal.

This process thus constructed a spatial map of the phase that the corrective pulse applies. Two sets of imaging data were acquired: the first experiment, where a corrective pulse contributes to the signal phase, and the baseline experiment, where it does not. Fourier transformation of the signals yielded two one-dimensional (1D) images. For each point in space, the difference between the phases of these two images then yielded the phase applied by the corrective pulse. Furthermore, deconvolution (by complex division in the time domain) of the spectral baseline removed the effect of the chemical shift on this image.

This technique verified two novel results: the combination of hardware matching effects with shim pulse effects and a third-order shim pulse that was translated by varying

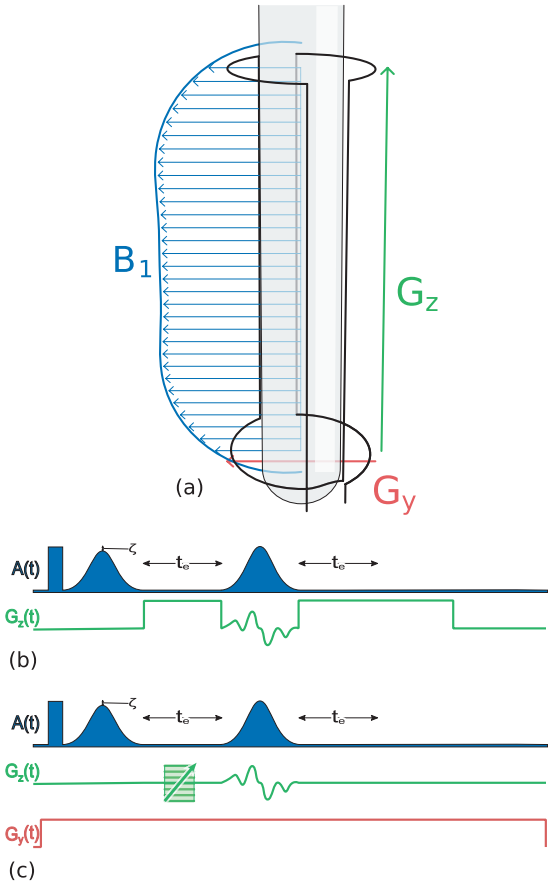

FIG. 4. (a) Schematic of the experimental setup, showing the direction of the applied gradients and rf field. (b) Pulse sequence for the 1D experiment, where different chemical shifts probe for offset robustness in a qualitative fashion. The adiabatic pulses are both amplitude (shown) and frequency (not shown) modulated. The gradient waveform consists of a waveform simultaneous with the rf pulse, for the shim pulse, in addition to a standard frequency encoding. Both these elements, as well as the rf amplitude scaling ζ, are removed for various reference scans, as explained in the text. (c) 2D pulse sequence, where an additional imaging gradient G_y directly probes offset robustness, while the phase encoding along the z direction provides an imaging dimension to map the phase applied along the z direction by the pulse.

amounts. Figure 5 plots the phase differences acquired by the experiments that verify the combination of matching and shimming. One experiment (shown in blue) demonstrates the phase applied by a simple matching pulse[24] and corresponds to the rf amplitude in the distorted imaging gradient field. The other experiment (shown in violet) demonstrates the first combination of rf-derived corrective effects with nonlinear imaging gradient-derived (i.e., shim pulse) effects in a single ADP. Finally, an experiment determined the phase of the corresponding shim pulse—without matching effects; the resulting phase was subtracted from that of the combined pulse to demonstrate that the residual phase can be attributed entirely to desirable matching effects (shown in red).

Figure 6 demonstrates the phase of a shim pulse, similar in effect to shim pulses previously generated.[25] This example, however, yields the first demonstration of a third-order correction and also demonstrates the coordinate-center translation of Eq. (12).

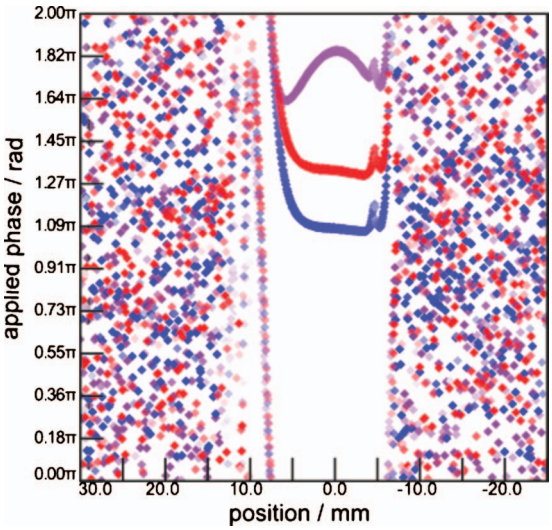

FIG. 5. Demonstration of the additive combination of matching and shimming in one dimension. The hardware-matching-only phase is plotted in blue, phase from the shimmed matching pulse is plotted in violet, and the difference between shimmed matching and shimming-only phases is plotted in red. (The intensity of the data points indicates the level of signal attenuation, with full opacity indicating no attenuation.) This demonstrates that the shimming and matching corrections can in fact be combined additively by a single pulse. Note that the location of the additive shim correction relative to the shimmed matching correction was adjusted through coordinate translation.

B. Two-dimensional example

To explicitly demonstrate the offset robustness of these pulses, as well as their versatility on different commercial systems, we ran experiments on a sample consisting of a mixture of 10% H_2O and 90% D_2O on a Varian Inova 300 MHz spectrometer. The rf field strength employed corresponded to a proton nutation frequency of approximately 8 kHz. As shown by Fig. 4(c), a gradient acted along the y direction for the duration of the experiment (except during the relaxation delay), and phase encoding replaced the frequency encoding of the 1D experiment. The reduced experiment time of the two-shot phase mapping method demonstrated here allows for the addition of an extra dimension. This extra dimension provides a precise demonstration of the pulses' insensitivity to offset, as shown in Figs. 7(a)–7(c). For completeness, and to verify that the shim pulse waveforms employed were the waveforms required by the simulations, the k-space trajectory of the gradient waveform was mapped by phase encoding on the same channel without the simultaneous application of the rf waveform.

V. SIMULATIONS

These experimental demonstrations of the effects of shimmed matching pulses allow us to better simulate their performance in a mobile MR setup and to address some problems that may arise in their application. We focus on the results from the two-dimensional (2D) experiment for two reasons. Primarily, these experiments explicitly ensure that the pulses will act uniformly over the given offset range. Much lower power ($\approx$1/10) rf pulses were also used in this experiment; the pulses are therefore longer and represent a greater challenge in terms of relaxation during the pulse.

Three separate resonance frequencies, separated appropriately for proton chemical shifts at 10 MHz, were chosen. The simulation of Figs. 8(a) and 8(b) focused on the ability of a shim pulse to correct inhomogeneities under these circumstances. It compared the resulting chemical shift spectrum under three different situations: evolution in a homogeneous environment with standard T_2 relaxation, evolution under an inhomogeneous field with an inhomogeneity suitable for correction by the phase shown in Fig. 7(c), and evolution without the effects of the inhomogeneous field but with an added period of relaxation for each acquisition point. The first situation corresponds to signal acquired in a homogeneous magnetic field, the second situation corresponds to signal acquired in an inhomogeneous field without correction, and the final situation corresponds to signal in the same inhomogeneous field, corrected by a pulse with only the z^2 shim portion of the phase experimentally demonstrated in Sec. IV [Fig. 7(c)].

The sum of a set of 1000 signals corresponding to evolution under fields offset by 0–6 ppm of z^2 inhomogeneity

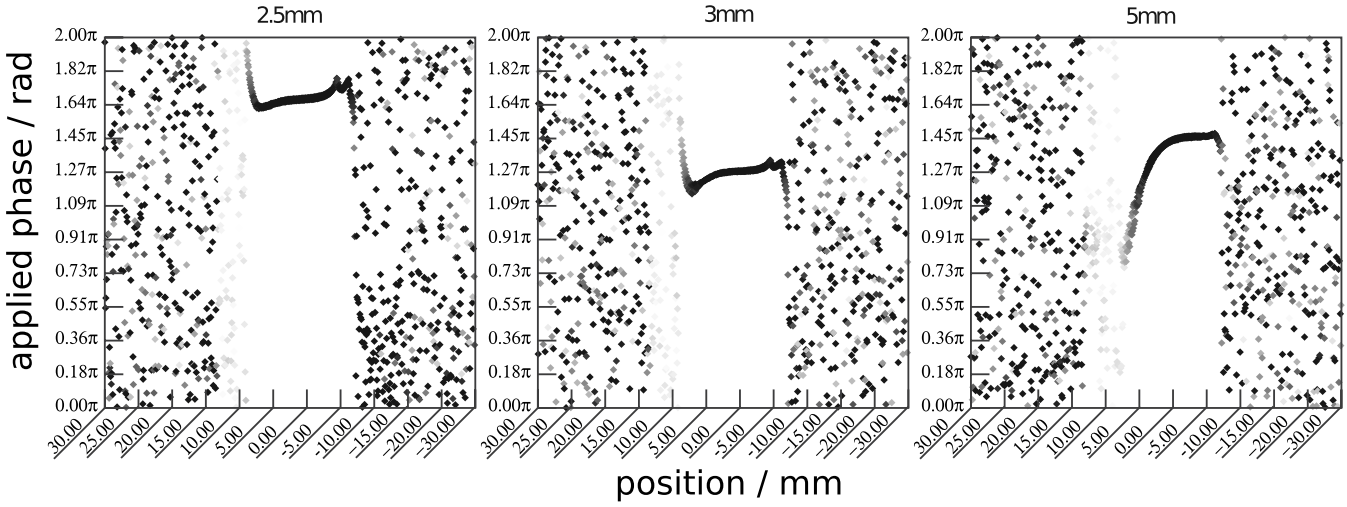

FIG. 6. A demonstration of a z^3 shaped shim pulse, which also demonstrates the use of Eq. (12) to translate the center of the applied phase by three different values.

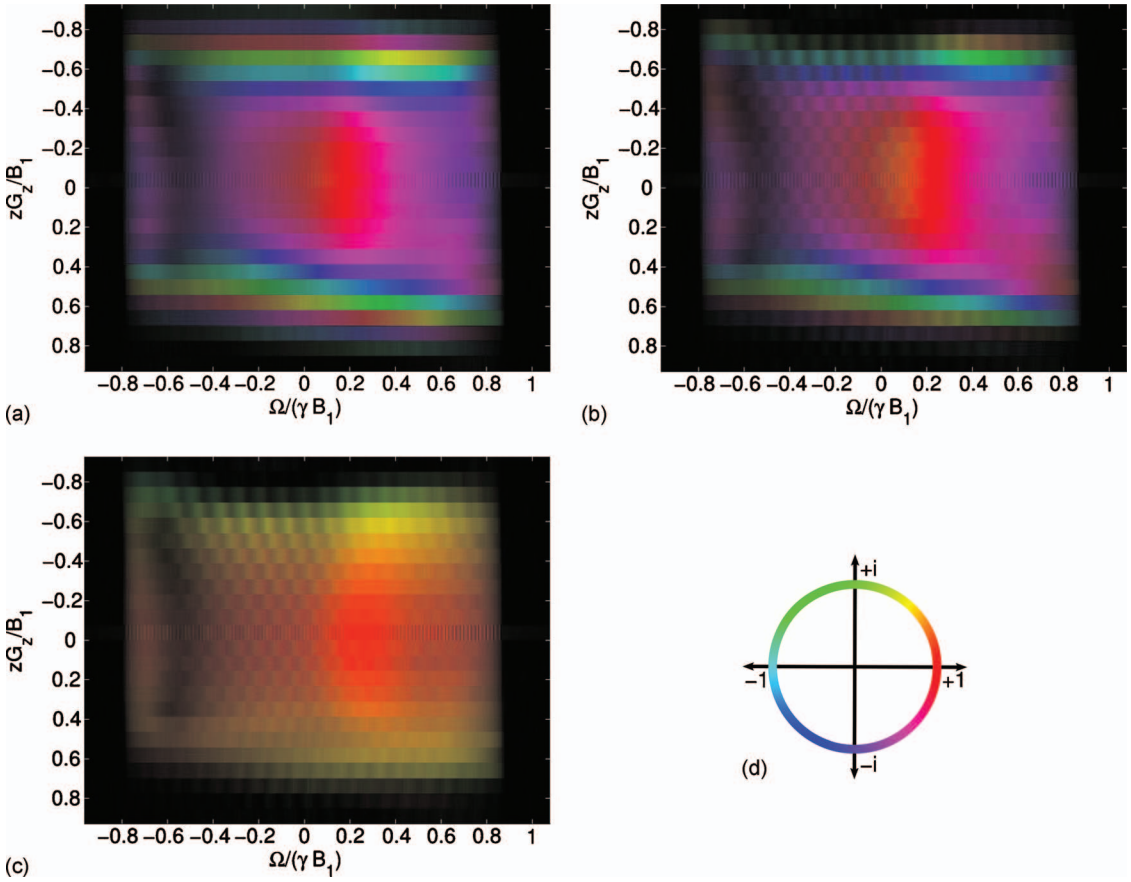

FIG. 7. The experiment of Fig. 4(c) was run with both the corrective (i.e., shim, matching, or shimmed matching pulses) and unaltered versions of the ADP. The resulting phase difference, plotted as variations in color (d), is mapped as a function of both the spatial z-coordinate and the local offset frequency. The experimental results shown here demonstrate both matching (a) and its combination with a second-order shim pulse (b) in an offset robust fashion. Plot (c) demonstrates that when the phase applied by the rf matching-only pulse is subtracted from the phase applied by the combined shimmed matching pulse, a pure parabolic shimming phase remains over an 8 kHz bandwidth. In these plots, the intensity of the pixels represents the intensity of the image signal, while the colors indicate the phase encoded by the corrective pulses. The units of both the static gradient strength and the local field offset are given relative to the magnitude of the rf field.

approximated the inhomogeneous signal. The additional relaxation during the corrective pulse was conservatively approximated as an additional period of T_2 relaxation (without chemical shift evolution) as long as the pulse length. At a longer T_2, simulations predict the recovery of signal by the corrective pulses [Fig. 8(a)]. The simulations also highlight a problem that occurs in the event of faster T_2 values: the relaxation during the corrective pulse overwhelms the signal recovery due to the correction [Fig. 8(b)].

Thus, these simulations underscore a fundamental limitation of adiabatic ex situ correction pulses in general (including those types previously published); namely, in order to recover more signal from rephasing than they lose due to relaxation, the pulses must supply a sufficiently large correction within a sufficiently short time. This relation, phrased succinctly in terms of the pulse length t_{pulse}, the time constant for relaxation during the pulse T_p, time between acquisitions t_{dw}, and the time constant for the decay the inhomogeneity imposes on the signal envelope[32] $T_2^{\dagger}$, becomes

$$\frac{t_{\text{pulse}}}{T_p} < \frac{t_{\text{dw}}}{T_2^{\dagger}}. \tag{16}$$

Note that T_p will remain roughly similar for all ADPs, meaning that the success of a corrective pulse will rely primarily not on the absolute strength of the correction applied, but on the product of t_{pulse} and $T_2^{\dagger}$ or, equivalently, the average rate at which the pulse applies the corrective phase. For any situation that satisfies Eq. (16), additional signal can always be recovered. On the other hand, when this condition is violated, the dephasing due to relaxation will always exceed the rephasing supplied by the corrective pulses, and can never be recovered, regardless of the acquisition scheme or the absolute length or strength of the pulses applied. Figures 8(b) and 8(d) [as compared with Figs. 8(c) and 8(a)] demonstrate an example of this inability to recover signal.

Finally, Figs. 8(c) and 8(d) demonstrate, on the one hand, how the addition of hardware matching effects can allow the pulses to correct for significantly greater inhomogeneity; in this example, an additional inhomogeneity of 0–27 ppm dephases the spins along a direction orthogonal to z and is compensated by a phase the same order of magnitude as the hardware matching phase of Fig. 7(a). On the other hand, these simulations also demonstrate how a pulse that employs only hardware matching results in a signal significantly inferior to that resulting from the combination of matching and shimming effects in the same pulse.

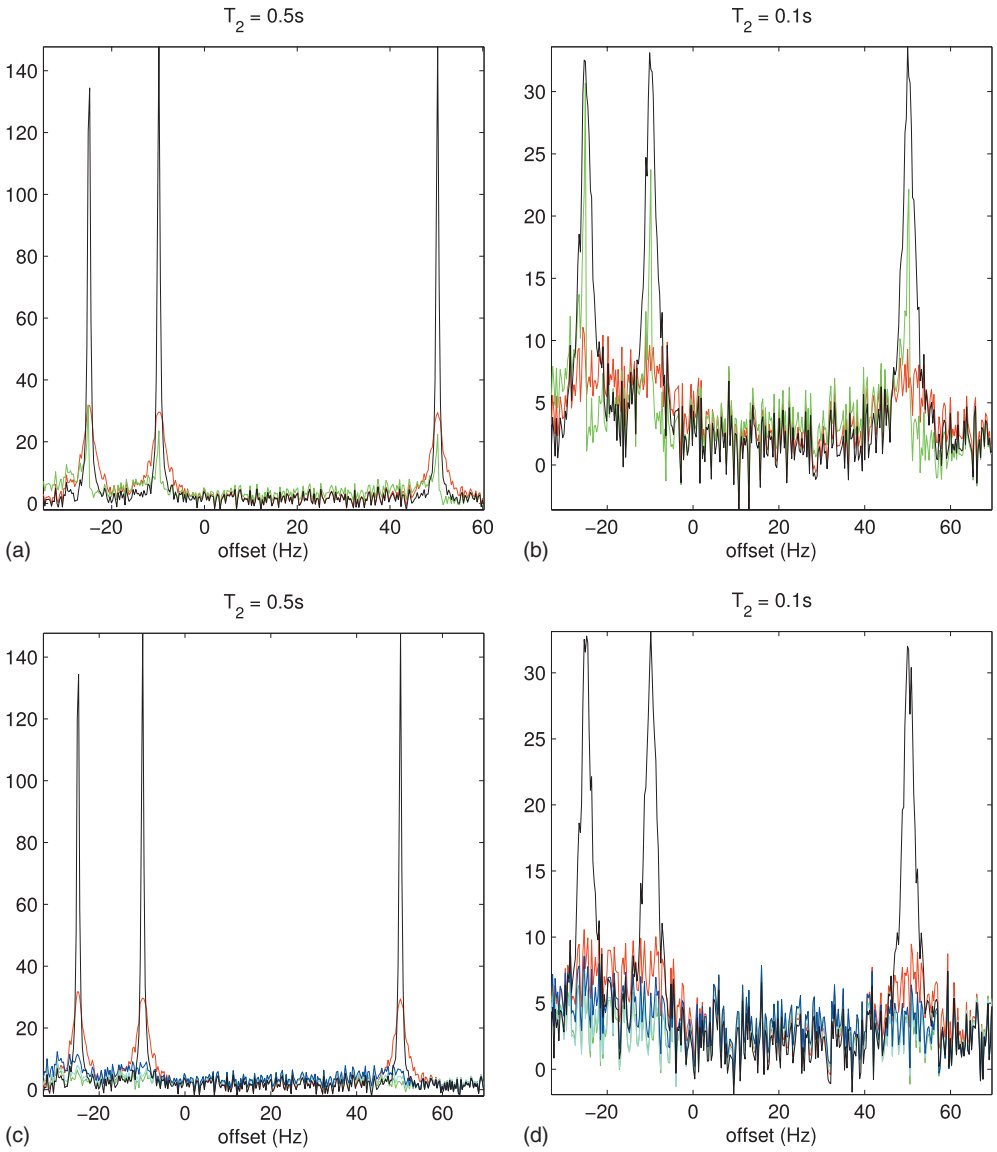

FIG. 8. Simulation of stroboscopic correction for two different relaxation time constants. The black, green, and red lines, respectively, represent simulations of spectra taken in a homogeneous field, an inhomogeneous field, and in an inhomogeneous field with correction. The top figures only incorporate a z^2 inhomogeneity, while the lower figures also incorporate a linear x inhomogeneity 9/2 as large, intended for correction by hardware matching methods. In the lower figures, the additional blue line represents a partial correction (incorporating matching but not shim pulse corrections), while the red line represents the full shimmed matching correction. Note how the shimmed matching correction gives dramatically more signal to noise and resolution than the matching-only correction, despite the fact that the maximum rotation supplied by the shimming correction is significantly smaller than that given by the matching correction. Note also how both the upper and lower figures demonstrate how relaxation during the pulses can compete with the pulses' ability to refocus the signal.

VI. QUANTIFICATION OF PULSE PERFORMANCE

Various researchers have previously simulated and applied a variety of robust corrective pulses.[24,25,33,34] Given the fact that various different acquisition schemes with various different strengths and weaknesses have been presented (e.g., stroboscopic correction versus correction along an indirect dimension),[16,17,20,33] and one can choose the optimal scheme for a given application from among these, one would also like to compare the amount of chemical shift resolution attainable with the different types of pulses. Unfortunately, such a direct comparison is not possible. The rotations applied by corrective pulses do not scale with increasing field strengths, as do chemical shifts, and so the same correction will provide a more meaningful gain in terms of chemical shift resolution at lower field. This issue, as well as the issue of the scaling of J-couplings,[20] has been addressed by previous publications. However, the performance of a specific type of corrective pulse will also vary greatly depending on the details of the experimental setup, and this issue has not been addressed.

The existing literature does not present the performance of corrective pulses in terms of units that allow a uniform comparison between different pulse types implemented in different experimental setups. However, by employing experiments (like those presented in Sec. IV of this paper) to collect a set of performance measures in the proper units, as outlined in this section, one can predict the amount of signal recovery possible with a given type of corrective pulse under a wide variety of different experimental conditions.

The following analysis develops naive measures of the

strength of the correction and of the pulses' robustness into what we term as the "corrective rate performance parameter" and "bandwidth performance parameter." It concludes with additional measures of the efficiency with which these pulses take the applied gradient strengths available and employ them to generate such corrections. Afterward, we apply this analysis to pulses previously presented in the literature, as well as the pulses presented here.

A. Initial analysis

The size of the corrective rotation (in radians, degrees, or cycles) will determine the strength of the correction applied by a corrective pulse, i.e.,

$$\varphi_{\max} = t_{\mathrm{dw}} \gamma \Delta B_{0,\max}. \tag{17}$$

(The maxima are maxima across the volume of the sample.) Here, φ is the strength of the corrective pulse, which can correct t_{dw} of inhomogeneous evolution in a field with inhomogeneity ΔB_0.

The bandwidth of offsets over which the pulse acts uniformly, $\Delta\Omega$, provides an equally (or more) important measure of the pulse's performance. In the absence of relaxation and diffusion, the successive repetition of an offset-independent pulse could achieve arbitrarily large corrections; in this limit, the size of the net correction would be limited by the bandwidth of the pulse rather than its corrective strength.

B. Uniform field scaling

In reality, relaxation and diffusion in the presence of a gradient do occur during a pulse. As demonstrated in Sec. V, this irreversible attenuation competes with the ability of a corrective pulse to refocus signal. A shorter pulse will, therefore, be more generally desirable. Corrective strength and bandwidth, as described above, neglect this important point and so do not suitably measure pulse performance.

A simple manipulation can aid the search for shorter pulses by predictably and arbitrarily reducing the length of any composite pulse. Specifically, a uniform scaling of $1/t_{\mathrm{pulse}}$ and the fields applied during a pulse $(\Omega/\gamma, B_1, \mathbf{r}\cdot\mathbf{G})$ will leave the resulting net rotation unchanged. This "uniform field scaling" will play a central role in our characterization of pulses.

The literature already routinely refers to the relative offset bandwidth Q_Ω,

$$Q_\Omega = \frac{\Delta\Omega}{\gamma B_{1,\max}}. \tag{18}$$

This remains constant during uniform field scaling and is important because it is limited for most kinds of rf pulses. However, in the case of adiabatic pulses, it is not limited, as longer pulses can give larger relative offset bandwidths. For instance, one can easily double the total relative bandwidth of an adiabatic pulse; by taking twice the amount of time to sweep over that bandwidth, the adiabaticity, and therefore, the fidelity of the pulse, remains constant. Therefore, we also refer to relative bandwidth sweep rate, $\Delta\Omega/\gamma B_{1,\max} t_{\mathrm{pulse}}$.

Similarly, uniform field scaling also preserves the angle of the corrective rotation $\varphi(\mathbf{r}\cdot\mathbf{G}/B_{1,\max})$ at each value of the relative gradient strength, $\mathbf{r}\cdot\mathbf{G}/B_{1,\max}$. However, the repetition of any corrective pulse will also amplify the corrective rotation; therefore, as already alluded to by Eq. (16), we will find it more interesting to refer to the corrective rate, $\varphi(\mathbf{r}\cdot\mathbf{G}/B_{1,\max})/t_{\mathrm{pulse}}$.

C. Limited rf amplitude

As previously stated, certain types of pulses will not be able to exceed a specific relative offset bandwidth, and so it will remain a useful measure of pulse performance. We develop two more standardized measures of pulse performance by noting that shorter pulses require correspondingly larger power to reproduce the same effect as longer pulses. The maximum rf power available will, therefore, limit the minimum pulse length, which in turn limits the bandwidth sweep rate and corrective rate.

Dividing the angle of corrective rotation by this minimum pulse length and subsequently finding the ratio to the available rf amplitude yields the (dimensionless) corrective rate performance parameter

$$P_{\mathrm{corr}} = \frac{\varphi(\mathbf{r}\cdot\mathbf{G}/B_{1,\max})}{\gamma B_{1,\max} t_{\mathrm{pulse}}}, \tag{19}$$

which, in concert with the bandwidth performance parameter

$$P_\Omega = \frac{\Delta\Omega}{\gamma^2 B_{1,\max}^2 t_{\mathrm{pulse}}}, \tag{20}$$

most accurately quantifies the ability of a given pulse shape to correct for inhomogeneities under a variety of experimental circumstances, where different amounts of rf power are available (Table III).

It is interesting to note that although we have not called upon adiabaticity in the derivation of these performance parameters, the same concepts used to derive offset independent adiabaticity[8] will lead to the conclusion that the bandwidth performance parameter (after incorporation of an additional offset to $\Delta\Omega$ to accommodate any gradients applied during the pulse) remains preserved for offset independent pulses of similar adiabaticity.

For the interested reader, an example, for the case of stroboscopic pulses, detailing how performance parameters could be included into a calculation of the impact of corrective pulses on the signal is included in the Appendix.

D. Efficiency

Finally, a simple measure of corrective rate performance will not suffice for some purposes, since its maximum magnitude will scale with the strength of the applied gradients available. Rather, one may require a measure of the efficiency with which pulses utilize the available applied gradient strength in order to generate corrective phase.

Although this work focuses on the development of adiabatic corrective pulses, even in the nonadiabatic case, the individual rotations (i.e., pulse slices) that contribute to a gradient-based (i.e., "shim pulse" type) correction do not depend on $\mathbf{r}$ and $\mathbf{G}/B_{1,\max}$ except as the product $\mathbf{r}\cdot\mathbf{G}/B_{1,\max}$.

TABLE III. The various quality measures remain constant under uniform field scaling. In order to express the desirability of shorter pulses, they can be converted into rates by dividing by the pulse length. Finally, they can be converted to performance parameters by normalizing out the available rf strength of the given experimental setup. The various order terms of P_{corr} give the efficiency of the gradient usage.

Quality measures		Rates	Performance parameters
Corrective strength	$\varphi_{\max}\left(\frac{\mathbf{r}\cdot\mathbf{G}}{B_{1,\max}}\right)$ [rad]	$\frac{\varphi_{\max}\left(\frac{\mathbf{r}\cdot\mathbf{G}}{B_{1,\max}}\right)}{t_{\mathrm{pulse}}}$ [rad/s]	$P_{\mathrm{corr}}=\frac{\varphi_{\max}\left(\frac{\mathbf{r}\cdot\mathbf{G}}{B_{1,\max}}\right)}{\gamma B_{1,\max}t_{\mathrm{pulse}}}$
Relative offset bandwidth	$Q_{\Omega}=\frac{\Delta\Omega}{\gamma B_{1,\max}}$	$\frac{\Delta\Omega}{\gamma B_{1,\max}t_{\mathrm{pulse}}}$ [s^{-1}]	$P_{\Omega}=\frac{\Delta\Omega}{\gamma^2 B_{1,\max}^2 t_{\mathrm{pulse}}}$ [rad^{-1}]
Efficiency			$\frac{1}{N!}\frac{\partial^N P_{\mathrm{corr}}}{\partial(\mathbf{r}\cdot\mathbf{G}/B_{1,\max})^N}=\frac{\varphi_N(\mathbf{r}\cdot\mathbf{G}/B_{1,\max})B_{1,\max}^{N-1}}{(\mathbf{r}\cdot\mathbf{G})^N\gamma t_{\mathrm{pulse}}}$

Therefore, their composite effect can be broken down into a series similar in form to Eq. (7) (although the general case will depend nonlinearly on time). The corrective rate performance parameter will depend on $\mathbf{r}\cdot\mathbf{G}/B_{1,\max}$ as

$$\frac{\varphi\left(\frac{\mathbf{r}\cdot\mathbf{G}}{B_{1,\max}}\right)}{\gamma B_{1,\max}t_{\mathrm{pulse}}}=\left(\frac{\mathbf{r}\cdot\mathbf{G}}{B_{1,\max}}\right)^N\underbrace{\left(\frac{\varphi\left(\frac{\mathbf{r}\cdot\mathbf{G}}{B_{1,\max}}\right)B_1^{N-1}}{\gamma(\mathbf{r}\cdot\mathbf{G})^N t_{\mathrm{pulse}}}\right)}_{N\text{th order efficiency}}$$

$$=\left(\frac{\mathbf{r}\cdot\mathbf{G}}{B_{1,\max}}\right)^N\frac{1}{N!}\frac{\partial^N P_{\mathrm{corr}}}{\partial\left(\frac{\mathbf{r}\cdot\mathbf{G}}{B_{1,\max}}\right)^N}. \qquad (21)$$

Assuming a pulse is designed to supply only an Nth order monomial term, $(\partial^N P_{\mathrm{corr}}/\partial(\mathbf{r}\cdot\mathbf{G}/B_{1,\max})^N)$ is a constant. In truth, this analysis ignores the presence of competing spatial monomial terms and spatial-offset cross terms and, therefore, the decreased fidelity of a pulse at higher gradient strengths. However, despite this, the appropriate Nth order coefficient (i.e., the "Nth order efficiency") measures how efficiently the pulse employs the available relative gradient strength to generate the desired monomial term and serves as an accurate measure of efficiency.

E. Application to specific methods

Here, we give an example of our standardization by applying it to previous corrective methods as well as the methods presented here. The original demonstration of shim pulses employed pulses with a total length of 1 ms at a B_1 strength corresponding to a proton 90° pulse width of 10 μs and a gradient strength of ≈0.025 T/m across ±0.5 cm, to give a phase change of 1 rad.[25] The first three quantities convert to a maximum relative gradient field strength of 0.21 and a pulse length corresponding to 157.08 rad of proton nutation at the maximum rf strength. This gives a corrective rate performance parameter of 6.4×10^{-3} and a second-order gradient efficiency of 0.14. The offset bandwidth is designed to be ±3.5 kHz, corresponding to a relative offset of 0.14; therefore, the pulses operate uniformly across a relative bandwidth performance parameter of 1.78×10^{-3} rad^{-1} (see Table IV for a summary of performance parameters listed in this section).

By comparison, the original simulations of adiabatic hardware matching pulses employ a total pulse length of 32 ms to give a z-rotation that differs by 100 rad between 5 and 20 kHz γB_1.[24] The pulse applies this phase uniformly over an offset bandwidth of ±50 kHz. Taking the maximum rf strength as the nominal rf strength, this corresponds to a corrective rate of 2.5×10^{-2} over a bandwidth performance parameter of 2.48×10^{-3} rad^{-1}. Thus, we have determined that, where the rf field falls off to zero, these pulses, which are chosen conceptually, without the need for computer optimizations, will supply phase at a faster rate than a fully optimized shim pulse. This remains true regardless of the total rf power available to the system.

Similarly we reference these more recent methods against composite z-rotation pulses,[16] which apply a z-rotation that varies by 22 rad as γB_1 ranges from 15 to 18 kHz; these rotations are applied consistently over an offset range of ±15 kHz. The pulse length in this case will correspond to 25 rad of proton nutation,[35] giving a corrective rate of 0.88. This, together with the bandwidth performance parameter of 3.6×10^{-2} rad^{-1}, indicates that these pulses utilize time rather efficiently. However, they were abandoned

TABLE IV. The corrective rate performance parameter and relative bandwidth performance parameter of, respectively, basic composite z-rotation pulses, the original demonstration of adiabatic hardware matching pulses, the original demonstration of shim pulses, and the shim portion of the shimmed matching pulses presented here. Note that z-rotation pulses are also limited to a relative offset bandwidth of 0.90.

	Corrective rate, P_{corr}	Bandwidth performance, P_{Ω}
z-rotation pulses	0.88	3.6×10^{-2} rad^{-1}
Hardware matching pulses	2.5×10^{-2}	2.48×10^{-3} rad^{-1}
Grid-optimized shim pulses	6.4×10^{-3}	1.78×10^{-3} rad^{-1}
Pulses optimized on-the-fly	1.8×10^{-3}	2.9×10^{-3} rad^{-1}

since they were fundamentally limited to a relative offset—in this case 0.90—which is far less than the relative offset of 5/2 given for this example of the adiabatic hardware matching pulses. The importance of the need for a completely flat offset dependence whose bandwidth can increase with increasing pulse length cannot be overemphasized for the case of strongly inhomogeneous systems.

Finally, the pulses demonstrated here have a net pulse length of 703.72 rad of proton nutation and generate a phase change of 1.26 rad per pulse, which corresponds to a corrective rate performance parameter of 1.8×10^{-3}. The relative gradient strength was approximately 0.7 at maximum, which indicates an efficiency of 3.0×10^{-3} while generating the second-order correction. These pulses exhibit insensitivity to offset over a range of $\Omega/\gamma B_1=\pm0.6$, which corresponds to a bandwidth sweep rate of 2.9×10^{-3} rad^{-1}. See Table IV for a summary of comparison of this to the performance of other ex situ pulses.

VII. DISCUSSION

MR systems with inhomogeneous fields have proven increasingly valuable, as they offer increased portability at dramatically diminished costs relative to traditional systems. Two strategies can correct the effects of these inhomogeneities and allow recovery of chemical shifts and, thus, a fully functional MR implementation. The first method, that of correcting field inhomogeneities by means of hardware shims, has recently proven very successful in specific applications.[5] An alternative strategy, which employs customized pulse sequences to achieve such corrections, could lead to a more robust and widely applicable method for recovering chemical shifts, as it relies on a minimal number of hardware components. This strategy met with initial success in model systems[16,25] and in systems with additional hardware shimming.[17] However, the design of improved pulse sequences proved nontrivial. As a result, after initial rapid success, the further advancement of corrective pulse methods designed for ex situ applications has slowed somewhat due to a perceived lack in the power or flexibility of corrective pulses, a lack of common understanding of the physical processes involved, the complexity of the optimization procedures involved, and concern over the routine application of such pulses on realistic spectrometer systems.

In order to justify the full characterization of practical inhomogeneous systems and implementation of corrective pulses on such systems, we have developed pulses tailored to the demands of portable systems and fully characterized their performance on a standard spectrometer system. These improved methods have the potential to meet these demands and overcome the obstacles facing current corrective pulses. We have demonstrated how increased physical insight can dramatically simplify the computations that calculate such pulse waveforms. More importantly, however, we have demonstrated an improved corrective scheme, which combines the power of adiabatic matching pulses with the flexibility of shim pulses.

Matching corrections can reduce the effective linewidth in a standard single-sided system from hundreds of kilohertz down to tens of, or even a single, kilohertz over volumes on the order of 1 mL; however, even in a 0.2 T system, this amazing improvement of one to two orders of magnitude still leaves several thousands of parts per million inhomogeneity. The method demonstrated here, however, can manipulate the adjustable, spatially nonlinear corrections of shim pulses to tweak the shape of the correction and eliminate the relatively small, yet crucial, remaining inhomogeneity. As Fig. 8(c) clearly demonstrates, the addition of a shimming correction can cause a profound difference in the signal to noise of the recovered hardware matching spectrum, despite the fact that the nonlinear shimming effects remain quite weak relative to the linear matching effects.[36]

In addition to this important step forward, these pulses exhibit the equally important benefits of robustness to changes in local field offset and a gradient field center position that can be easily shifted across space. The shift in the coordinate center will be particularly necessary in single-sided systems, where the center of the applied gradient coordinates does not necessarily fall within the sample. The built-in offset dependence of these pulses, meanwhile, sets them apart from other methods of pulse-based correction (e.g., Refs. 9 and 20). When attempting the application of corrective pulses to full-volume, highly inhomogeneous systems, the offset robustness of pulses is by far the most difficult and also the most important parameter to improve. Nonetheless, we have demonstrated a rather simple and conceptual procedure for achieving such an offset independence, even in the presence of complicated spatial phases.

Aside from directly addressing the previously mentioned issues, this work also clearly demonstrates the limitations of pulse-based inhomogeneity corrections: they are inherently order based. As a result, more complex spatial corrections require either more complex hardware, stronger fields, or longer pulse lengths. To uniformly express how far we can push these limits, we have clarified parameters to characterize the performance of pulses implemented under a variety of experimental conditions. We note that the performance of the pulses presented here is reduced from that of grid-optimized pure shim pulses (where the phase is iteratively calculated at various points on a spatial grid and optimized[25]). In order to accommodate an on-the-fly optimization, small gradient amplitudes have been used in order to eliminate higher order terms, and the waveform is not further optimized, thus compromising the efficiency of the pulse. The combination with matching pulses also implies some loss in efficiency, since the gradients act only during a single full passage and because the optimization must also eliminate high-order mismatch terms.

Of course, successive improvements in the corrective rate and offset dependence of corrective pulses will serve to further improve these pulses. The conceptual model and means for quantifying pulse performance developed here lay firm groundwork for such studies. Most notably, this strategy is compatible with a more traditional grid-based optimization. Although we have demonstrated that on-the-fly optimization is possible and that the gradient waveforms need not be constrained to a sum of basis functions, increased efficiency may be more important for a particular application. In

that case, one could represent the gradient waveform with a basis set,[25] and then optimize over the subspace orthogonal to the undesired terms. Such a strategy could only improve upon the efficiency exhibited by the current methodology, while maintaining the same combination of features. Most importantly, future work with these methods will include full characterization of a portable system, so that we might design, adapt, and implement such corrections on that system.

Overall, we have presented a simple and direct strategy for combining a variety of features into a single corrective pulse. This makes these pulses more suitable for application to truly portable ex situ systems. The combination of correction strength and correction accuracy, the improvement in the pulse optimization rate, and the enhanced ability to experimentally characterize pulse performance demonstrated here are all critical steps toward the implementation of an adjustable, robust correction of inhomogeneities by means of rf pulses. A step has certainly been made toward a system of pulse-based inhomogeneity correction that is both practical and general. Significantly, this step has been made based on models and physical understanding rather than raw simulation power. Furthermore, we believe that the application of the types of pulses developed here is not limited to that of corrective pulses and could have implications touching on the fields of ultrafast NMR spectroscopy and MR imaging.

ACKNOWLEDGMENTS

This work was supported by the Director, Office of Science, Office of Basic Energy Sciences, Materials Sciences and Engineering Division, of the U.S. Department of Energy under Contract No. DE-AC02-05CH11231. We would also like to acknowledge Dr. Sabieh Anwar for helpful commentary on this manuscript.

APPENDIX: ANALYTICAL CALCULATION OF SIGNAL CORRECTION BASED ON PERFORMANCE PARAMETERS

In general, we are interested in resolving the sum of various spectral components that constitute a NMR signal $s_h(t)$. We start by assuming that this signal is normalized to a maximum amplitude of 1. In the absence of relaxation, such a signal would not decay. However, even in a perfectly homogeneous field, relaxation broadens the peaks of the spectrum, resulting in a finite linewidth.

Postprocessing techniques, such as deconvolution, can, in principle, improve the resolution of the spectrum. However, the fact that the relaxation restricts the signal within a "signal envelope" of finite energy

$$E_{\mathrm{env}} = \int_0^\infty \exp\left(-\frac{2t}{T_2}\right) dt \tag{A1}$$

will impose a limit on the net signal energy generated by the sample

$$E = \int_0^\infty \exp\left(-\frac{2t}{T_2}\right) |s_h(t)|^2 dt. \tag{A2}$$

Because a set background of noise always accompanies the signal, the limited signal energy will frustrate any efforts to recover resolution by postprocessing.

Therefore, focusing on determining the resulting signal energy, we now include the effects of corrective pulses in an inhomogeneous field. When the sample generates signal from within an inhomogeneous field, that field will have the effect of multiplying the homogeneous signal by the additional envelope $e_{\mathrm{inh}}(t)$,

$$e_{\mathrm{inh}}(t) = \frac{1}{V}\int e^{i\gamma\Delta B_0(\mathbf{r})t} d\mathbf{r}. \tag{A3}$$

Meanwhile, we note that a corrective pulse will correct for some field shape, which may or may not be the same as the field shape which determines e_{inh} (for instance, the latter is the case for a matching pulse in a realistic inhomogeneous field which does not also employ shimming corrections); therefore, it will effectively divide the signal by an envelope $e_{\mathrm{corr}}(t)$, which may or may not be the same as $e_{\mathrm{inh}}(t)$. As discussed in Sec. VI, every corrective pulse will also subject the signal to additional randomized dispersion, which introduces an additional decay $e_{\mathrm{stoch}}(t)$, which cannot be removed by any means. Furthermore, variation in the pulse rotation at different local field offsets will result in a distortion and attenuation of the signal in the frequency domain, which in turn will be manifest as a convolution of the time domain signal. We denote the convolution kernel resulting from this distortion by $d(t)$; although we denote the offset dependent effects here as a time-domain convolution for compactness, their effect can be more conveniently thought of as a frequency-dependent attenuation of the signal before correction. Therefore, the total energy of the corrected signal will be exactly

$$E = \int_0^\infty \left| ((e_{\mathrm{inh}} e_{\mathrm{free}} s_h) * d) \frac{e_{\mathrm{stoch}}}{e_{\mathrm{corr}}} \right|^2 dt, \tag{A4}$$

where e_{free} is the dispersion due to relaxation and diffusion during the period of free evolution. In words, as a generalization of Eq. (16), signal recovery will result when, on average, the envelope of the inhomogeneity decay that the

pulse corrects for (e_{corr}) decays more rapidly than the envelope of attenuation due to the relaxation and diffusion introduced by the pulse (e_{stoch}); this statement is not limited to the case of stroboscopic acquisition. Of course, this equation also highlights the need for a pulse with sufficient offset robustness to avoid signal attenuation due to the convolution by d.

If we take into account relaxation during the pulses T_p, during a stroboscopic sequence, we obtain

$$e_{\text{stoch}}(t) = \exp\left(-\frac{r_{\text{pulsing}} t_{\text{pulse}} t}{T_p}\right), \tag{A5}$$

where t_{pulse} gives the pulse length and $r_{pulsing}$ gives the number of pulses applied stroboscopically per unit acquisition time. We can also incorporate the effects of diffusion if we assume that the static field gradient is greater than the applied field gradients and approximate it by a constant value g_{inh}. Approximating the adiabatic passages as instantaneous inversions,[37] we then obtain

$$e_{\text{stoch}}(t) = \exp\left(-\frac{r_{\text{pulsing}} t_{\text{pulse}} t}{T_p} - \frac{1}{48} D r_{\text{pulsing}} t \gamma^2 g_{\text{inh}}^2 t_{\text{pulse}}^3\right), \tag{A6}$$

where D gives the self-diffusion constant.

The corrective rate performance parameter P_{corr}, in conjunction with the rf amplitude available in a given experimental setup $B_{1,max}$, will determine the amount of time required by the corrective pulses (i.e., $r_{pulsing} t_{pulse} t$) per unit free evolution time t, namely,

$$r_{\text{pulsing}} t_{\text{pulse}} = \frac{\Delta B_{0,\max}}{B_{1,\max} P_{\text{corr}}}, \tag{A7}$$

where $\Delta B_{0,max}$ gives the maximum field inhomogeneity across the sample. Although it is very important to note that offset-dependent distortions or attenuations will further complicate matters, we can at this point stop to note the resolution gains possible from such a correction, namely,

$$\frac{\Delta f_{\text{corrected}}^{-1}}{\Delta f_{\text{uncorrected}}^{-1}} = \left(1 + \frac{(\Delta B_{0,\max}/P_{\text{corr}} B_{1,\max})(1/T_p + 1/48\,\gamma^2 D g_{\text{inh}}^2 t_{\text{pulse}}^2) + 1/T_{2,\text{residual}}^{\dagger}}{1/3\,\gamma^2 g^2 t^2 + 1/T_2 + 1/T_2^{\dagger}}\right)^{-1}, \tag{A8}$$

where we have defined the resolution Δf^{-1} as proportional to the time constant of the decay of a signal envelope and where $T_{2,residual}^{\dagger}$ gives the time constant for the decay of the envelope corresponding to e_{inh}/e_{corr}; we note that this can be very large for an accurate correction such as a shimmed matching pulse, but significantly smaller for a hardware-matching-only correction employed in a realistic environment.

Finally, we can incorporate the parameters to describe offset performance. For an idea of how this would work, let us approximate the offset dependence as full correction over the bandwidth of the pulse, and no signal elsewhere. Then

$$d = \int e^{i2\pi f t} H(2\pi f - \gamma^2 P_{\Omega} B_{1,\max}^2 t_{\text{pulse}}) df, \tag{A9}$$

where $H(x)$ is 1 for $|x| \leq 1/2$ and 0 elsewhere. In this approximation, signal from regions with inhomogeneity greater than the pulse bandwidth will simply be lost, resulting in signal attenuation. However, distortions can be significantly more complicated.

We note that although the above analysis holds for the specific case of a stroboscopic acquisition, we hope that it helps both to satisfy the curiosity of those interested in the effects of diffusive attenuation and to provide an example for the straightforward application of uniform performance parameters toward predicting the amount of signal/resolution recovery in indirect acquisition schemes.[5,33]

[1] B. Blümich, J. Perlo, and F. Casanova, Prog. Magn. Res. Spec. **52**, 197 (2007).
[2] R. Kleinberg, A. Sezginer, D. Griffin, and M. Fukuhara, J. Magn. Reson. **97**, 466 (1992).
[3] V. Demas, J. Herberg, V. Malba, A. Bernhardt, L. Evans, C. Harvey, S. Chinn, R. Maxwell, and J. Reimer, J. Magn. Reson. **189**, 121 (2007).
[4] A. McDowell and N. Adolphi, J. Magn. Reson. **188**, 74 (2007).
[5] J. Perlo, F. Casanova, and B. Blumich, Science **315**, 1110 (2007).
[6] R. Tycko, Phys. Rev. Lett. **51**, 775 (1983).
[7] D. Zax and S. Vega, Phys. Rev. Lett. **62**, 1840 (1989).
[8] A. Tannús and M. Garwood, J. Magn. Reson., Ser. A **120**, 133 (1996).
[9] N. Khaneja, T. Reiss, C. Kehlet, T. Schulte-Herbrüggen, and S. Glaser, J. Magn. Reson. **172**, 296 (2005).
[10] M. Hürlimann and D. Griffin, J. Magn. Reson. **143**, 120 (2000).
[11] E. Hahn, Phys. Rev. **80**, 580 (1950).
[12] S. Ahola, J. Perlo, F. Casanova, S. Stapf, and B. Blümich, J. Magn. Reson. **182**, 143 (2006).
[13] D. Weitekamp, J. Garbow, J. Murdoch, and A. Pines, J. Am. Chem. Soc. **103**, 3578 (1981).
[14] S. Vathyam, S. Lee, and W. Warren, Science **272**, 92 (1996).
[15] A. Maudsley, A. Wokaun, and R. Ernst, Chem. Phys. Lett. **55**, 9 (1978).
[16] C. Meriles, D. Sakellariou, H. Heise, A. Moule, and A. Pines, Science **293**, 82 (2001).
[17] J. Perlo, V. Demas, F. Casanova, C. Meriles, J. Reimer, A. Pines, and B. Blumich, Science **308**, 1279 (2005).
[18] Specifically, this refers to the phase of the I^+ density matrix element, or, equivalently, the signal phase as detected on a typical spectrometer.
[19] J. Pauly, P. Le Roux, D. Nishimura, and A. Macovski, IEEE Trans. Med. Imaging **10**, 53 (1991).
[20] B. Shapira and L. Frydman, J. Magn. Reson. **182**, 12 (2006).
[21] E. Kupce and R. Freeman, J. Magn. Reson., Ser. A **103**, 358 (1993).
[22] A. Tal and L. Frydman, J. Magn. Reson. **182**, 179 (2006).
[23] B. Shapira and L. Frydman, J. Am. Chem. Soc. **126**, 7184 (2004).
[24] C. Meriles, D. Sakellariou, and A. Pines, J. Magn. Reson. **164**, 177 (2003).
[25] D. Topgaard, R. Martin, D. Sakellariou, C. Meriles, and A. Pines, Proc. Natl. Acad. Sci. U.S.A. **101**, 17576 (2004).
[26] L. Bouchard and M. Anwar, Phys. Rev. B **76**, 014430 (2007).
[27] More correctly, they generate corrective phases at a much slower rate than hardware matching pulses.

[28] M. Garwood and L. DelaBarre, J. Magn. Reson. **153**, 155 (2001).
[29] S. Conolly, G. Glover, D. Nishimura, and A. Macovski, Magn. Reson. Med. **18**, 28 (1991).
[30] Generally, when we refer to "position" or **r**, we refer to the coordinate(s) along which the applied gradients vary.
[31] Note that all terms not containing ζ are the same for both adiabatic full passages and will cancel.
[32] Where we have used the notation $1/T_2^*=1/T_2+1/T_2^\dagger$, where T_2^* is the effective decay constant for the FID envelope. Note that when considering diffusion in the presence of a gradient, this relation becomes somewhat more complicated, as detailed in the Appendix.
[33] V. Demas, D. Sakellariou, C. Meriles, S. Han, J. Reimer, and A. Pines, Proc. Natl. Acad. Sci. U.S.A. **101**, 8845 (2004).
[34] D. Sakellariou, C. Meriles, A. Moulé, and A. Pines, Chem. Phys. Lett. **363**, 25 (2002).
[35] 22 rad+π rad for two $\pi/2$ pulses.
[36] Although we expect larger matching corrections to be achievable and useful in single-sided systems than in the typical spectrometer system demonstrated here, we note that this would only further obscure the (blue) partially corrected spectrum, rather than affecting the (red) fully corrected spectrum.
[37] D. Topgaard and D. Sakellariou, J. Chem. Phys. **125**, 044503 (2006).